

Characterization of the Factors Influencing Retained Austenite Stability in Q&P Steels *via In Situ* EBSD



D. ADAMS, M. BEHLING, M.P. MILES, E.R. HOMER, A.K. SACHDEV, E.V. WHITE, and D.T. FULLWOOD

The current work studies the correlations between microstructure and retained austenite (RA) transformation, in a single-quenched and partitioned (Q&P) 1180 steel microstructure, through *in situ* tensile tests combined with electron backscatter diffraction (EBSD) analysis. This allows the study of RA stability across a limited range of morphological characteristics to be studied in the absence of confounding factors introduced by varying the entire steel microstructure. Among the microstructural attributes of interest, RA grain aspect ratio is found to have the largest influence on transformation rate, where globular-shaped grains transform more slowly than those with a more lenticular shape. Furthermore, by tracking individual grains during deformation, it is apparent that larger grains transformed more slowly than smaller grains; a purely statistical study of grain size *vs* strain might conclude that smaller grains are more stable, but in reality, the smaller grains transform faster and are simply statistically replaced by partially transformed larger grains. These conclusions are in contrast to relationships that might be inferred from previous studies where the entire steel microstructure was varied, along with the morphology of the RA.

<https://doi.org/10.1007/s11661-023-06991-4>

© The Minerals, Metals & Materials Society and ASM International 2023

I. INTRODUCTION

IN the automotive industry, improving fuel efficiency of vehicles and decreasing greenhouse gas emissions are major objectives. One of the main strategies for achieving this goal is through lightweighting the body structure, while maintaining necessary strength and safety requirements. Lightweighting can be achieved by substituting light metals like aluminum for steel, or by downgauging—using stronger steels to provide the same structural integrity with thinner gage sheets. Third-generation advanced high strength steels (AHSS) use various tricks to provide higher strength, while retaining sufficient ductility to be formed into typical automotive components. One specific approach involves transformation induced plasticity (TRIP), where retained austenite (RA) is present in the room-temperature steel and facilitates higher ductility when it transforms to martensite during deformation. Recently, the development of quenched and partitioned (Q&P) steels,^[1–6] a third generation TRIP-based AHSS, has shown a very

promising balance between ductility and high strength, making it a candidate to replace some more traditional AHSS, like dual-phase (DP) steel. However, even higher gains might be possible if the microstructure-level contributors to rate of RA transformation (and related ductility increases) were better understood.

Q&P steels possess a complex microstructure, including RA grains, achieved through a unique heat-treating process. This process begins with the complete austenitization of the steel and then proceeds with the quenching of the steel below the martensite start temperature but above the martensite finish temperature. The alloy is held at this temperature, called the partitioning step, where carbon from the supersaturated martensite diffuses to surrounding austenite grains.^[2,7,8] The increased amount of carbon in the austenite gives it stability when the metal is then cooled to room temperature, resulting in various amounts of RA in the microstructure.^[9]

The presence of metastable RA, which transforms to martensite during subsequent deformation, has been correlated to an increase in alloy ductility *via* the TRIP effect. Furthermore, a gradual transformation of the RA with increasing strain is assumed to be ideal. Too rapid of a transformation of all the austenite would not contribute to ductility at later stages of deformation; on the other hand, incomplete transformation of the RA would reduce its effectiveness.^[10] Understanding the microstructural features that control the rate of RA transformation is, therefore, critical to improving ductility.

D. ADAMS, M. BEHLING, M.P. MILES, E.R. HOMER, and D.T. FULLWOOD are with the Brigham Young University, Provo, UT 84602. Contact e-mail: dfullwood@byu.edu A.K. SACHDEV is with the General Motors R&D, Warren, MI 48092. E.V. WHITE is with the University of Utah, Salt Lake City, UT 84112.

Manuscript submitted September 1, 2022; accepted January 22, 2023.

Article published online February 11, 2023

Various factors have been found to play a significant role in the stability of RA during deformation processes. These factors include (i) carbon content of the RA grains,^[10–18] (ii) RA grain size and morphology,^[10–15,17–22] (iii) crystallographic orientation,^[13,17] (iv) neighboring phases and grains,^[10,11,16,17,21–23] and (v) temperature at which the steel is strained.^[24,25] However, in most of these studies, characteristics of the RA are not varied independently of that of the surrounding phases; hence, relationships between RA properties and transformation rate can often not be inferred independently of the rest of the microstructure. For example, a majority of studies suggest that a higher carbon content increases the stability of the austenite grains,^[12,16,22,26] while another study that reviewed transformation in a single Q&P material found that lower carbon content within austenite can correlate with increased stability.^[18] While studying RA transformation in a single microstructure, across a range of deformation levels, may not provide data across the full range of possible RA characteristics, it does provide a much more controlled study of the influence of various traits on transformation rate.

This study seeks to identify correlations between transformation behavior and key characteristics of austenite grains within a single microstructure of Q&P 1180, observing the same region across a range of strain levels. Electron backscatter diffraction (EBSD) images of the samples are taken, and several hundred RA grains are tracked during *in situ* tensile deformation. Statistical analysis is performed to identify correlations between microstructural characteristics and RA stability. Linear regression is used to quantify the influence of the dominant attributes on the transformation rate, where an approximately linear relationship exists. Identifying these attributes and their influence on transformation rate will guide optimization of these AHSS for lightweighting applications.

II. METHOD

The material used in this study was a Q&P 1180 steel provided by Bao Steel, with composition given in Table I. The predominant phases are martensite, ferrite, and austenite. The original sheet had a nominal thickness of 1.2 mm; dog-bone-shaped tensile specimens, with gage length of 10 mm and width of 2 mm, were cut from the sheet keeping the tensile axis parallel to the rolling direction. Due to the force limitations of the *in situ* tensile stage used in this study, it was required that the dog-bone samples are grounded down to approximately 0.4 mm thickness, which was done using 60 grit polishing paper. Once final thickness was obtained, the samples were subsequently polished on the opposite side, to a grit size of 1200 fine following standard mechanical procedures. Each sample was then polished to a final state for EBSD using electro-polishing. For the electro-polishing, a solution of 125 ml methanol, 75 ml Butanol, and 25 ml Perchloric acid, kept at 10 °C,^[27] was used and samples were polished at approximately 20 V and 1.0 A for 24 seconds.

Table I. Q&P 1180 Chemical Composition (Percent Weight)

Supplier	Grade	C	Mn	Si
BAO	1180 Q&P - uncoated	0.19	2.8	1.6

After polishing, fiducial marks were made on the gage length of the samples using a Focused Ion Beam (FIB) to mill-distinguishing features on the surface of the sample. This allowed the same area to be found easily and quickly for multiple scans at different strain steps.

The EBSD data were acquired using a square scan grid at an accelerating voltage of 20 kV, working distance of 17 mm, tilt angle of 70 deg, and a magnification of $\times 8000$. Scan sizes were typically 17.5×17.5 mm, with a step size of 80 nm. Scans in each series were taken close to fiducial marks at the unstrained condition and in the same area for each strain step afterwards. To obtain concurrent local strain data, foreshatter images were also obtained at each strain step and used for digital image correlation (DIC) as outlined in Reference 28.

A cleanup routine was applied to the resulting EBSD data to reduce the amount of noise being interpreted as austenite grains. Figure 1 shows an original phase map compared to the cleaned map, where red is austenite and green is ferrite/martensite. The cleanup routine utilized was the neighbor pattern averaging re-indexing (NPAR) using OIM Analysis v 8.1, followed by grain dilation.^[29] NPAR improved the indexing success rate of the scans, and grain dilation eliminated grains of size 3 pixels or less. The same routine was applied to all scans in this study. As can be seen from Figure 1, many points along grain boundaries (GBs), which are the strings of small red dots on the pre-cleanup phase map, appear to have been misindexed in the original scan on the left—a common occurrence due to mixed patterns arising at GBs.

RA grains that remained after the initial cleanup were tracked during subsequent tensile strain steps. The transformation rate for each grain was determined by measuring the percent transformation for a given strain step, *i.e.*, the grain's original area minus its current area, divided by its original area, all multiplied by 100, and then dividing this by the amount of strain undergone for the current strain step. This was done for four total scan areas, using three different samples, resulting in 303 grains for detailed investigation to determine microstructural features that correlate with RA grain transformation rate. However, the smaller grains were still susceptible to noise—misindexing due to carbon buildup on the surface, sample surface deformation, and other factors meant that tracking the size of grains smaller than around $0.1 \mu\text{m}^2$ resulted in a signal-to-noise ratio that was unacceptable. Hence, grains in the original samples smaller than this size (*i.e.*, less than around 16 pixels) were not included in the statistical analysis, leaving 167 grains that were tracked at various strain steps up to 14 pct strain. Since there is a significant possibility that thin RA lathes occur in the same regions that are susceptible to noise (*i.e.*, along grain boundaries), RA grains with such thin morphology are unlikely to be captured using the current approach.

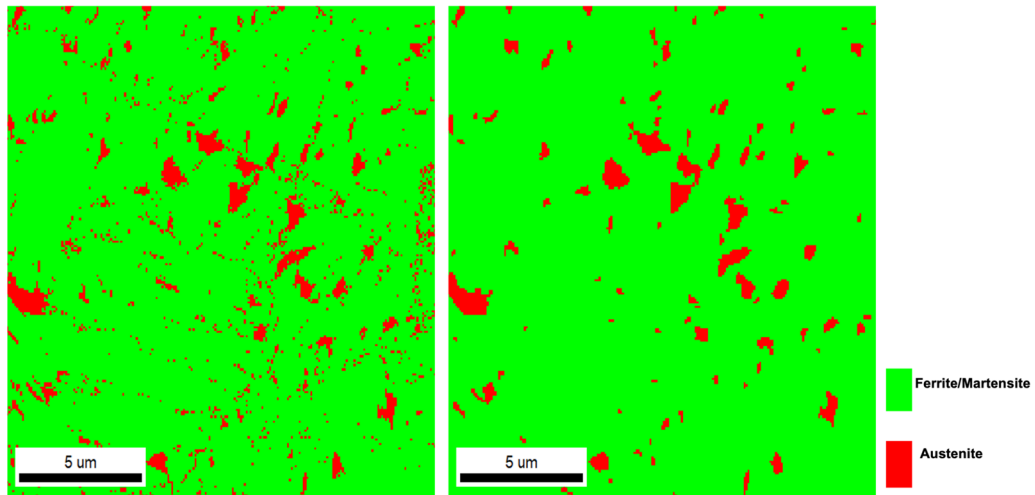


Fig. 1—Example effect of cleanup method on a phase map of one sample area. (Left) Phase map prior to cleanup. (Right) Phase map after cleanup.

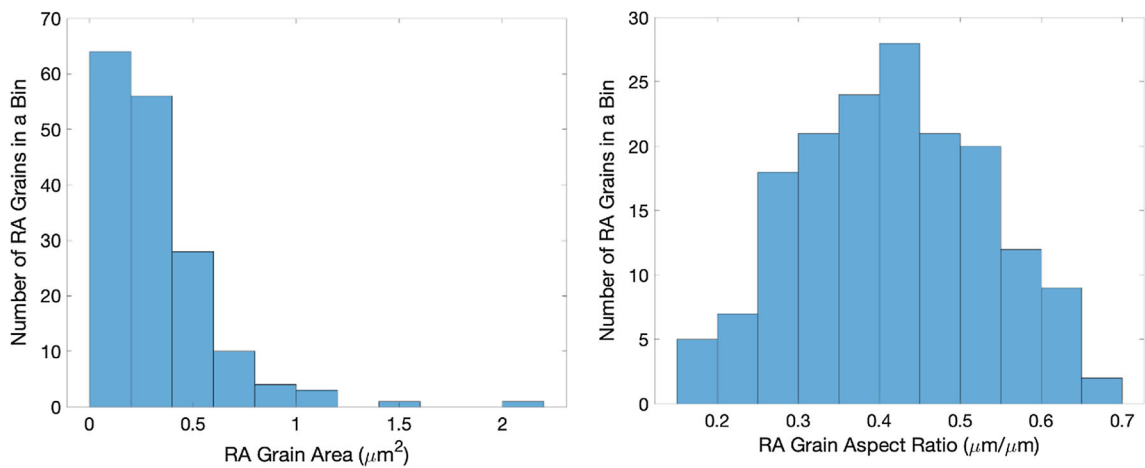


Fig. 2—Distribution of RA grain areas (left) and aspect ratios (right) for the 167 RA grains tracked in this study.

The grain data produced subsequent to cleanup were exported to a text file and a MATLAB script was used to extract the shape, orientation, size, surrounding phase, and Taylor factor, as reported by OIM. The distribution of size and aspect ratio of the 167 RA grains tracked in the rest of the study are shown in Figure 2. High-resolution EBSD was used to determine geometrically necessary dislocations (GND) density. The set of attributes used in the statistical studies was selected from a larger set used in a preliminary machine learning model, as reported in Reference 30; the six most promising attributes from that study are shown in Table II. RA grain orientations were approximately evenly distributed across orientation space, and GND content follows an approximately normal distribution around the mean of $277 \times 10^{12} \text{ m/m}^3$, and standard deviation of 66×10^{12} .

Even with the cleanup routine described above, not every RA grain that was tracked displayed a monotonic increase in percent transformation due to noise in the EBSD data; however, the trends across the full dataset were generally clear. In order to observe the correlation

between material attribute and transformation rate (transformation rate being equal to percent transformation divided by strain), a linear regression was performed on strain vs percent transformation. The ranges of selected features of RA grains (such as grain aspect ratio) were binned, and the fraction of total RA area in grains within a given bin was plotted against strain. A best-fit straight line was determined for the data from 0 to 10 pct strain using Matlab linear regression tool ‘fitlm’^[33]; since full transformation occurred for many grains by this strain level, the trend often became nonlinear beyond 10 pct. This resulted in a rate of transformation being measured for each bin of each feature. The standard error of regression was also calculated, and any points that were more than 2 standard errors away from the regression line were removed as outliers. Only two outliers were removed, and since they did not greatly affect the observed trend, it was assumed that they were mostly the result of misindexing as discussed earlier. The slopes of these regression lines are the transformation rates, having units of percent over strain. Regression analysis was then performed (again using the fitlm algorithm) to

Table II. List of Attributes Included in the Dataset with Corresponding Descriptions

Attribute	Description
Area	area of the grain in μm^2 ^[31]
Grain Aspect Ratio (GAR)	ratio of the minor axis to the major axis of the ellipse fit to the grain ^[31]
Major Axis Orientation (MAO)	angle in degrees of the major axis of the ellipse fit to the grain with respect to the tensile direction ^[31]
RA Taylor Factor (TF)	Taylor factor of RA grain calculated in OIM analysis relative to the tensile direction
Taylor Factor Difference (TF difference)	difference between the average Taylor factor of neighboring grains and the Taylor factor of the RA grain ^[32]
RA Grain GND Content (GND)	average GND value within an RA Grain at zero strain and calculated in OIM analysis. Units of 10^{12}

determine the correlation between a given attribute and the transformation rate, and to quantify P and R^2 values.

III. RESULTS

Figure 3 shows the Inverse Pole Figure (IPF), phase, and foreshatter detector (FSD) maps subsequent to cleanup for one of the samples scanned. The IPF maps show the gradual change in orientations of the grains as the sample is pulled in tension; the FSD images on the bottom show how the surface of the sample changed during deformation. Most relevant to this study, the phase maps show the transformation of the austenite grains as the strain is increased and the austenite disappears. Based on these images, transformation seems to occur in three different ways: gradually with deformation (see circled grains), rapidly at higher strains (see boxed grains), or not at all (see grains in triangles). Results of the regression analysis performed for various attributes vs transformation rate are presented in Table III.

The P value represents the probability that there is no correlation between the attribute and transformation rate given that the data collected are true. Thus, a P value below 0.05 indicates that a correlation between an attribute and transformation rate can be affirmed with 95 pct confidence. The R^2 value represents how much variation in transformation rate is explained by the attribute. Thus, a higher R^2 value indicates a stronger correlation between the attribute and transformation rate. Along with these values, the plots of transformation rate vs attribute provide visual insights into the relationships, as shown in Figure 4. Best-fit regression lines are shown for the attributes with significant correlations with the rate of transformation.

Figure 4(a) shows the results for the grain aspect ratio (GAR) attribute. As grain aspect ratio increases, the rate of transformation tends to decrease. Since the P value for this data is less than 0.05, a negative correlation between GAR and transformation rate can be confirmed at the 95 pct confidence level. This suggests that lamellar grains are less stable and transform more readily than the more globular-shaped grains, a conclusion also reached in Reference 13, but contrary to that found in References 10, 12, 16, 20, and 34. This apparent contradiction may be at least partially resolved by a

closer look at the studies. The paper by de Knijf *et al.* that agrees with the current study looks in detail at RA grains with a range of aspect ratio values, while the opposing studies generally categorize RA as having either a thin-film morphology or a blocky shape. For example, the thin-film RA grains in Reference 16 appear to have an aspect ratio of less than 0.1 which is lower than the range considered in this study. Furthermore, the thin films are likely to be associated with different relative positions within the microstructure, compared with blocky RA found in other steels—once again highlighting the issue of comparing behavior of RA across various microstructures. One potential explanation for lower stability of RA grains with low GAR is that the more slender grains have a higher probability of intersecting with a strain band, compared with more spherical grains. This is discussed in the context of the major axis orientation (MAO) of RA grains below. Based upon the high level of confidence arising from the statistics in the current study, it appears that, at least for the current Q&P steel, RA stability reduces with GAR, all other things being equal.

One way to quantify the impact each attribute has on transformation rate is to consider the slope of the regression line shown in Figure 4. Since each attribute has a significantly different range, the most meaningful measure relates to the difference between the transformation rates at the extreme values of the range for a given attribute. A larger difference indicates that, across the observed range of an attribute, there will be a larger change in transformation rate. The relevant values are shown in Table IV. As seen from the table, the transformation rate change across the range of observed GAR is 523 pct/strain; *i.e.*, by this measure, GAR has more than twice the impact on transformation rate than the other significant microstructure attributes (area and Taylor factor).

The most common attribute related to transformation, as studied in the literature, is grain size. Typically, large grains (greater than $1 \mu\text{m}^2$) are found to be unstable and transform quickly; small grains (less than $0.1 \mu\text{m}^2$) are the opposite and have a much higher stability, possibly not transforming at all.^[10,13,22,26,34] In this study, very small grains (less than $0.1 \mu\text{m}^2$) were not tracked, and hence, the stability of these grain cannot be ascertained. However, Figure 4(b) indicates fairly

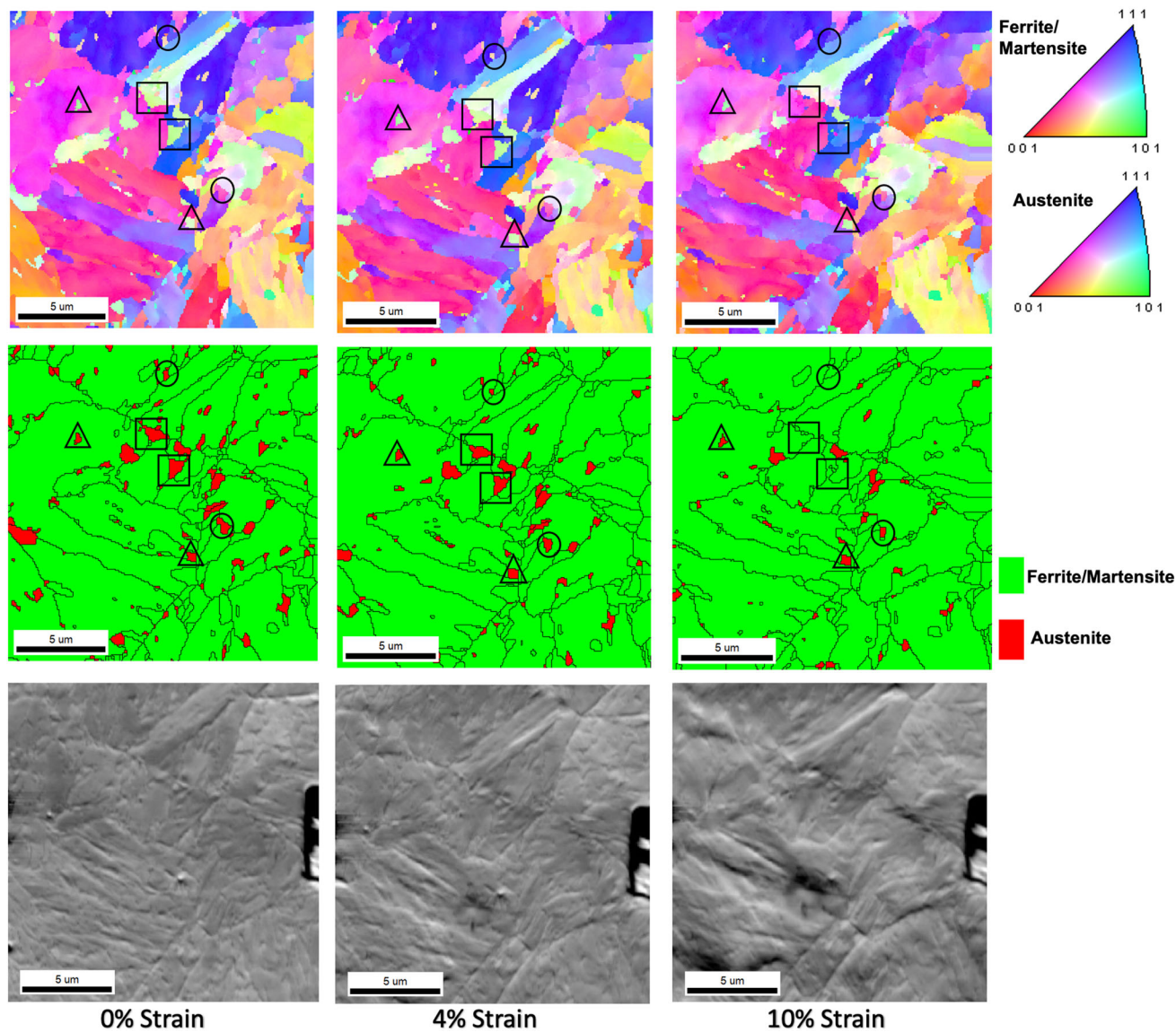


Fig. 3—IPF (top), Phase (middle), and FSD (bottom) maps of sample 1 area scanned using EBSD and strained *in situ*; three of the seven total strain steps are shown. Phase images are after cleanup routine described previously. The circled RA grains transform evenly with strain; those enclosed in a square are stable for low strains and transform rapidly at higher strains; those in triangles undergo negligible transformation.

Table III. P and R^2 Values for Given Attributes *vs* Transformation Rate Across All Strains

	GAR	Area	Taylor Factor	MAO	GND	TF Difference
P	0.01	0.08	0.02	0.55	0.343	0.125
R^2	0.63	0.42	0.78	0.06	0.0642	0.303

convincingly that, in general, as area increases, transformation rate tends to decrease. Since the P value for this data is 0.08, a negative correlation between area and transformation rate can be concluded with only 92 pct confidence, and hence, should be considered with care.

One potential reason for the difference in trends regarding area *vs* transformation rate between this and previous studies is illustrated in Figure 5. The plot quantifies the fraction of RA grains within each grain size bin as strain increases from 0 to 10 pct. Looking at

this figure, one might conclude that the larger grains transform most rapidly since the percentage of larger grains decreases with strain (in general the fraction of grains in the bins above $0.4 \mu\text{m}^2$ reduces with strain). However, in reality, the smaller grains transformed more rapidly but were statistically replaced by partially transformed larger grains. This would not be apparent if individual grains were not tracked during the entire deformation. Most studies in this area do not track individual grains but monitor the statistics of grain size.

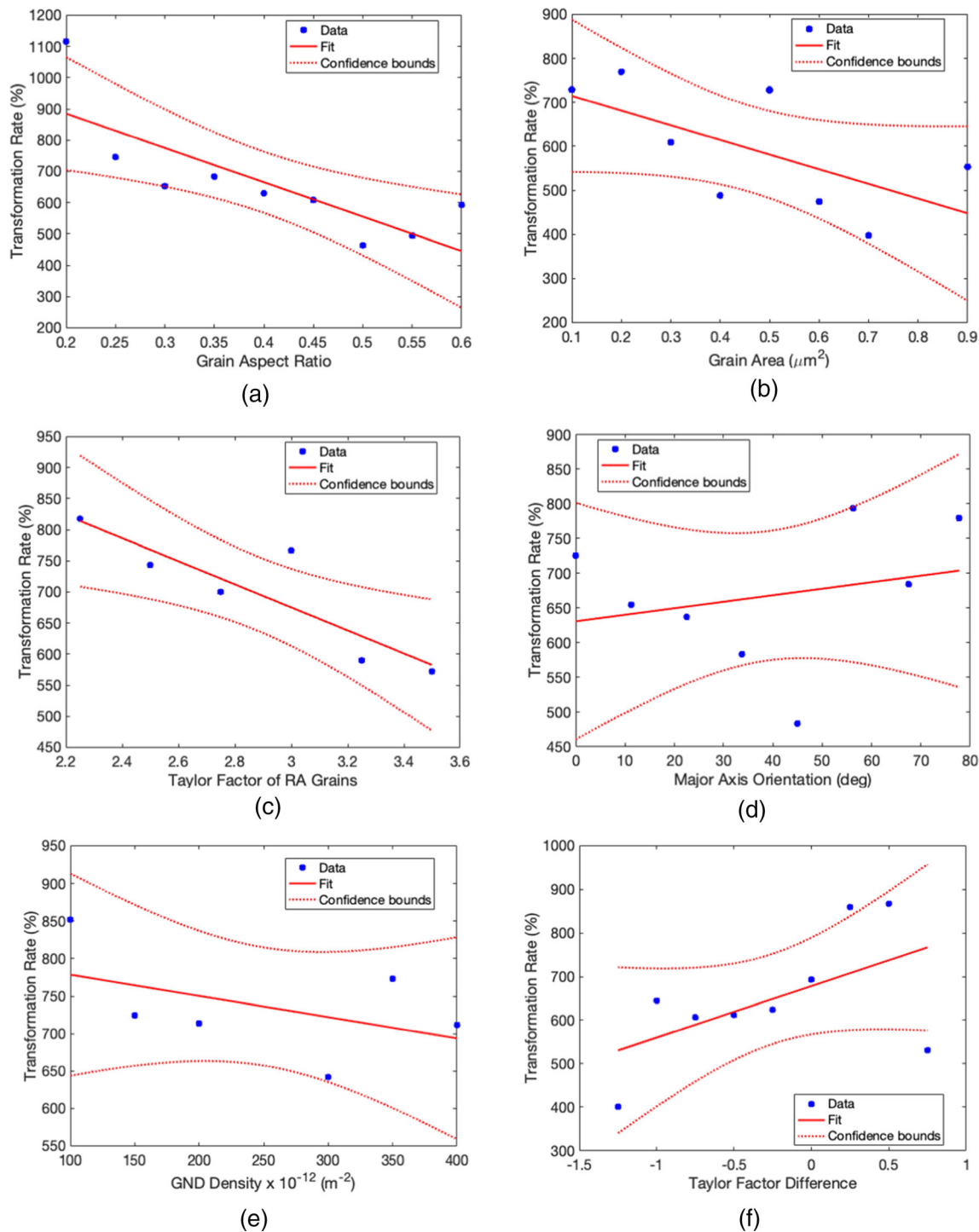


Fig. 4—Plots of rate of RA transformation vs (a) Grain Aspect Ratio, (b) Area, (c) Taylor Factor, (d) Major Axis Orientation, (e) Geometrically Necessary Dislocations, (f) Nearest Neighbor Taylor Factor Difference.

It should also be noted that the EBSD data obtained for this study provide only 2D images of the microstructure, meaning only a slice of the material's microstructure is analyzed. Therefore, it is impossible to tell which slice of a 3D grain has been captured, so the grains that are small enough to be considered stable and unlikely to transform could in reality be only the tip of a large grain underneath, in which case transformation should

happen quite readily. The problem of drawing conclusions about a 3D microstructure based on 2D results should, therefore, be considered throughout. Due to the large number of grains considered in the study and the statistical unlikelihood of this misrepresentation of grain size, however, this phenomenon is unlikely to significantly influence these results.

Table IV. Change in Transformation Rate Across the Range of each Attribute with a Significant Correlation

Material Attribute	Transformation Rate Change (Pct/Strain)
GAR	523
Area	176
Taylor Factor	246

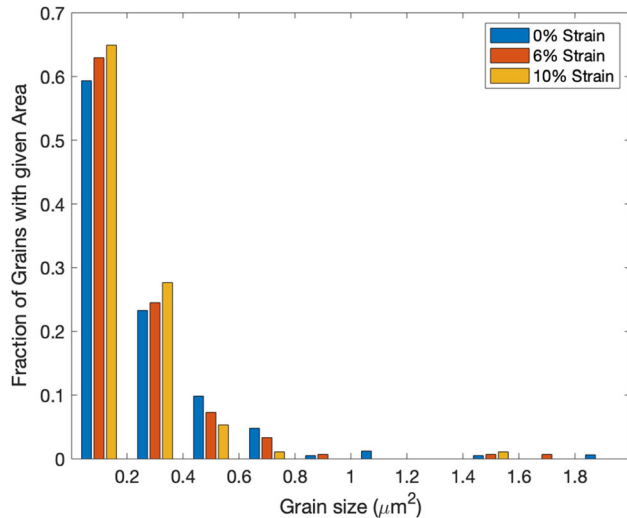


Fig. 5—The fraction of RA grains within each grain size bin as strain increases.

Taylor Factor also heavily influences transformation rate. Taylor Factor is similar to the Schmid Factor and gives the propensity of a crystal to slip, essentially becoming a multiplication factor on the yield stress; grains with lower Taylor Factor could, therefore, be termed “soft.”

Figure 4(c) supports this conclusion, indicating a negative correlation between Taylor Factor and transformation rate. Since the *P* value for this data is less than 0.05, a negative correlation can be concluded between transformation rate and Taylor Factor at the 95 pct confidence level. A microstructure consisting of RA grains with a higher Taylor Factor will, therefore, transform more slowly.

According to Table III, the normalized transformation rate difference for Taylor Factor is 246, the second largest difference of the attributes studied. In addition to the strong negative correlation between Taylor Factor and transformation rate, Taylor Factor has a strong effect on transformation rate.

There is no noticeable correlation between major axis orientation (MAO) and transformation rate as seen in Figure 4(d). The high *P* value suggests that a linear correlation cannot be concluded with any significant amount of confidence. Despite not suggesting a linear correlation, the data in Figure 4(d) suggest the possibility of a bimodal correlation between transformation rate and major axis orientation. The decision similarly predicted transformation below 41 and above 57 deg but not between the two. A potential explanation for this bimodal trend lies in shear bands. These occur at 45 deg from the

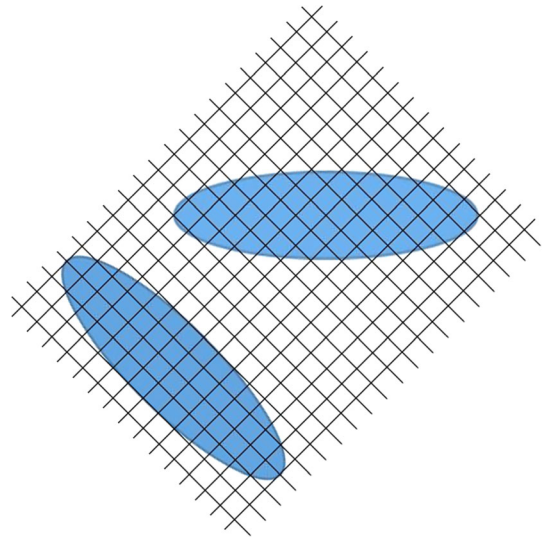


Fig. 6—Illustration of shear bands (lines) and the difference in number of intersection points between grains oriented at 0 and 45 deg to the horizontal, or loading direction. The grain on top (MAO = 0 deg) has approximately 43 intersection or nucleation points and the other grain (MAO = 45 deg) has only about 30.

loading direction, and the intersection of these bands with the austenite grain is typically assumed to provide nucleation sites for the transformation event. Therefore, when the grains are oriented at 45 deg to the loading direction already, the number of intersections, or nucleation sites, is less than when the grain is at 0 or 90 deg. Figure 6 helps illustrate this hypothesis, where the lines represent the shear bands and the ovals represent the RA grains. The grain with MAO of 0 deg has 43 shear band intersections with the grain boundary while the grain with MAO of 45 deg has 30 shear band intersections.

As shown in Figure 4(e), there appears to be a weak negative correlation between RA Grain GND and transformation rate. However, since the *P* value for this data is very high (0.343), no correlation can be concluded between them with any significant amount of confidence. A previous study found a positive correlation between percent transformation and GND^[35] but did not consider transformation rate.

The effect of neighboring grains’ “hardness” on RA transformation, quantified in the attribute TF Difference, has been studied in past research, but the conclusions reached are different. Some suggest that harder surrounding phases prevent transformation by limiting the volume increase accompanied by transformation,^[10,16,18] while others say that the harder phases propagate stress directly to the RA, causing it to transform quicker.^[22,36,37] It is important to note that in this study, a negative value for Neighboring Grain Taylor Factor Difference means that the grain that is being observed has a higher Taylor Factor, or is harder than the neighboring grains; in other words, TF difference is calculated by subtracting Taylor Factor of the observed grain from the average Taylor Factor of the neighboring grains.

Figure 4(f) indicates that there is not a linear correlation between TF difference and transformation rate. The graph shows a general upward trend, but the *P*

value of 0.125 is too high to conclude a positive correlation with 90 pct confidence or more. In other words, a positive correlation between Nearest Neighbor Taylor Factor Difference is possible but cannot be concluded in this research.

IV. CONCLUSIONS

The goal of this work was to assess the influence of microstructural characteristics on transformation rate of near-surface RA grains in Q&P 1180 steel. Individual grains were tracked by EBSD in a single material during *in situ* tensile deformation. Hence, correlations between microstructural attributes and RA stability could be inferred without the complication of modifying the surrounding microstructure to arrive at different RA morphologies, as has been done in many previous studies. Furthermore, this allowed more accurate assessment of transformation rate compared with other studies; if individual grains are not tracked, then it will not be clear whether smaller grains are more stable, or (as is apparent from the current study) small grains transform first, but are statistically replaced by partially transformed larger grains.

One hundred and sixty seven grains with size above 0.1 mm² were analyzed; the aspect ratios observed did not include fine lathes that have been studied in several previous publications. Furthermore, the 3D morphology was not captured by the surface EBSD, potentially leading to some of the noise in the data. Nevertheless, the statistical trends will be valid.

A statistical analysis was performed on these same attributes by quantifying the transformation rate of grains across the range of values of a given characteristic. The key findings at the 90 pct confidence level are the following:

1. Increases in RA grain aspect ratio, grain area, and Taylor Factor all have the effect of slowing transformation rate.
2. GAR has the strongest effect on transformation rate, followed by Taylor factor, and then RA grain area.
3. No linear correlations were found between transformation rate and RA grain major axis orientation, GND content, and TF difference with neighboring grains, although nonlinear relationships may exist.

These observations suggest characteristics of microstructures for Q&P 1180 that might be explored in order to increase ductility.

ACKNOWLEDGMENTS

This work was supported by the National Science Foundation grants DMR 1507095 and CMMI 1926662. Thanks to Jeff Cramer for his help with the initial sample preparation.

DATA AVAILABILITY

The data required to reproduce these findings are available to download from: <https://data.mendeley.com/drafts/mm4g75jvsp>.

CONFLICT OF INTEREST

On behalf of all authors, the corresponding author states that there is no conflict of interest.

REFERENCES

1. E. De Moor, S. Lacroix, A.J. Clarke, J. Penning, and J.G. Speer: *Metall. Mater. Trans. A*, 2008, vol. 39A, pp. 2586–95.
2. D.V. Edmonds, K. He, F.C. Rizzo, B.C. De Cooman, D.K. Matlock, and J.G. Speer: *Mater. Sci. Eng. A*, 2006, vol. 438, pp. 25–34.
3. M.J. Santofimia, L. Zhao, R. Petrov, C. Kwakernaak, W.G. Sloof, and J. Sietsma: *Acta Mater.*, 2011, vol. 59, pp. 6059–68.
4. M.J. Santofimia, L. Zhao, and J. Sietsma: *Metall. Mater. Trans. A*, 2009, vol. 40A, pp. 46–57.
5. J. Speer, D.K. Matlock, B.C. De Cooman, and J.G. Schroth: *Acta Mater.*, 2003, vol. 51, pp. 2611–22.
6. L. Wang and J.G. Speer: *Metallogr. Microstruct. Anal.*, 2013, vol. 2, pp. 268–81.
7. A.J. Clarke, J.G. Speer, M.K. Miller, R.E. Hackenberg, D.V. Edmonds, D.K. Matlock, F.C. Rizzo, K.D. Clarke, and E. De Moor: *Acta Mater.*, 2008, vol. 56, pp. 16–22.
8. J.G. Speer, D.K. Matlock, L. Wang and D. Edmonds: in *Comprehensive Materials Processing*, S. Hashmi, B.G. Ferreira, C.J. Van Tyne, and Y. Bekir, eds., Elsevier, 2014, pp. 217–25.
9. M.J. Santofimia, L. Zhao, and J. Sietsma: *Metall. Mater. Trans. A*, 2011, vol. 42A, pp. 3620–26.
10. J. Chiang, J.D. Boyd, and A.K. Pilkey: *Mater. Sci. Eng. A*, 2015, vol. 638, pp. 132–42.
11. A. Basuki and E. Aernoudt: *J. Mater. Process. Technol.*, 1999, vol. 90, pp. 37–43.
12. J. Chiang, B. Lawrence, J.D. Boyd, and A.K. Pilkey: *Mater. Sci. Eng. A*, 2011, vol. 528, pp. 4516–21.
13. D. De Knijf, C. Fojer, L.A.I. Kestens, and R. Petrov: *Mater. Sci. Eng. A*, 2015, vol. 638, pp. 219–27.
14. E. Jimenez-Melero, N.H. van Dijk, L. Zhao, J. Sietsma, S.E. Offerman, J.P. Wright, and S. van der Zwaag: *Scripta Mater.*, 2007, vol. 56, pp. 421–24.
15. J.B. Seol, D. Raabe, P.P. Choi, Y.R. Im, and C.G. Park: *Acta Mater.*, 2012, vol. 60, pp. 6183–99.
16. Y.F. Shen, L.N. Qiu, X. Sun, L. Zuo, P.K. Liaw, and D. Raabe: *Mater. Sci. Eng. A*, 2015, vol. 636, pp. 551–64.
17. G.K. Tirumalasetty, M.A. van Huis, C. Kwakernaak, J. Sietsma, W.G. Sloof, and H.W. Zandbergen: *Acta Mater.*, 2012, vol. 60, pp. 1311–21.
18. X.C. Xiong, B. Chen, M.X. Huang, J.F. Wang, and L. Wang: *Scripta Mater.*, 2013, vol. 68, pp. 321–24.
19. Z.H. Cai, H. Ding, R.D.K. Misra, and Z.Y. Ying: *Acta Mater.*, 2015, vol. 84, pp. 229–36.
20. I. de Diego-Calderon, D. De Knijf, M.A. Monclus, J.M. Molina-Aldareguia, I. Sabirov, C. Fojer, and R.H. Petrov: *Mater. Sci. Eng. A*, 2015, vol. 630, pp. 27–35.
21. W.S. Li, H.Y. Gao, H. Nakashima, S. Hata, and W.H. Tian: *Mater. Charact.*, 2016, vol. 118, pp. 431–37.
22. I.B. Timokhina, P.D. Hodgson, and E.V. Pereloma: *Metall. Mater. Trans. A*, 2004, vol. 35A, pp. 2331–41.
23. P.J. Jacques, J. Ladriere, and F. Delannay: *Metall. Mater. Trans. A*, 2001, vol. 32A, pp. 2759–68.
24. R. Blonde, E. Jimenez-Melero, L. Zhao, J.P. Wright, E. Bruck, S. van der Zwaag, and N.H. van Dijk: *Acta Mater.*, 2012, vol. 60, pp. 565–77.
25. X.D. Wang, B.X. Huang, Y.H. Rong, and L. Wang: *Mater. Sci. Eng. A*, 2006, vol. 438, pp. 300–05.

26. Q. Zhou, L.H. Qian, J. Tan, J.Y. Meng, and F.C. Zhang: *Mater. Sci. Eng. A*, 2013, vol. 578, pp. 370–76.
27. G.K. Tirumalasetty: in *Kavli Institute of Nanoscience*. Delft University of Technology, 2013.
28. D. Adams, S. Irfan, J. Cramer, M.P. Miles, E.R. Homer, T. Brown, R.K. Mishra, and D.T. Fullwood: *Microsc. Microanal.*, 2020, vol. 26, pp. 641–52.
29. S.I. Wright, M.M. Nowell, S.P. Lindeman, P.P. Camus, M. De Graef, and M.A. Jackson: *Ultramicroscopy*, 2015, vol. 159, pp. 81–94.
30. D. Adams: in *Mechanical Engineering*. Brigham Young University, Provo, 2019.
31. OIM Analysis 8.0: EDAX, 2016.
32. M. Knezevic, B. Drach, M. Ardeljan, and I.J. Beyerlein: *Comput. Method Appl. M.*, 2014, vol. 277, pp. 239–59.
33. MATLAB: The Mathworks, Inc., 2022.
34. A.F. Mark, X. Wang, E. Essadiqi, J.D. Embury, and J.D. Boyd: *Mater. Sci. Eng. A*, 2013, vol. 576, pp. 108–17.
35. R. Sharma, C.M. Poulin, M. Knezevic, M.P. Miles, and D.T. Fullwood: *Mater. Sci. Eng. A*, 2021, vol. 825, pp. 76–87.
36. P.J. Antony, P. Manujesh, and N.A. Jnanesh: in *Recent Trends in Electronics, Information & Communication Technology (RTEICT)*, *IEEE International Conference on*, IEEE, 2016, pp 69–73.
37. D. De Knijf, R. Petrov, C. Fojer, and L.A.I. Kestens: *Mater. Sci. Eng. A*, 2014, vol. 615, pp. 107–15.

Publisher's Note Springer Nature remains neutral with regard to jurisdictional claims in published maps and institutional affiliations.

Springer Nature or its licensor (e.g. a society or other partner) holds exclusive rights to this article under a publishing agreement with the author(s) or other rightsholder(s); author self-archiving of the accepted manuscript version of this article is solely governed by the terms of such publishing agreement and applicable law.